

EFFECT OF PRE-HEAT TREATMENT ON CORROSION BEHAVIOR OF NICKEL-ALUMINIUM BRONZE ALLOY

M.R. Daroonparvar¹, M. Mazar Atabaki^{2,3*}, A. Vakilipour³

¹*Department of Materials Engineering, Faculty of Mechanical Engineering,
Roudehen Branch, Islamic Azad University, Roudehen, Tehran, Iran*

²*Institute for Materials Research, the School of Process, Environmental and
Materials Engineering, Faculty of Engineering, University of Leeds, Leeds, UK*

³*Department of Materials Engineering, Faculty of Mechanical Engineering,
Universiti Teknologi Malaysia, 81310, Malaysia*

Received 06.06.2011

Accepted 19.09.2011

Abstract

The effect of microstructure of nickel-aluminum bronze alloy (NAB) on the corrosion behavior in artificial seawater is studied using linear polarization and impedance tests. The alloy was heat treated in different heating cycles including quenching, normalizing and annealing. Microstructure of the specimens was characterized before and after heat treatment by optical microscopy and scanning electron microscopy. Results showed that the fraction of pearlite phase in the normalized alloy is much more than other specimens, leading to higher corrosion resistance. Polarization test showed that starting point of passivation in the polarization of the normalized alloy is lower than other specimens. The dissolution of Mn and Fe rich phases increased the Mn and Fe contents in solid solution, and this enhanced the passivation power of the surface of the alloy. The effect of the alloying elements was seen by a lower corrosion potential and an inflexion at around 280 mV (SCE) in the polarization curve, indicating the preferential dissolution of some elements beyond that potential.

Key words: Nickel-aluminum bronze alloy; Heat treatment; Corrosion; Microstructure

Introduction

Nickel-aluminum bronze known as NAB is a series of copper-based alloy with additions of 9-12% Al and 6% Ni and Fe. High corrosion resistance of this alloy has

* Corresponding author: M. Mazar Atabaki, pmmmaa@leeds.ac.uk

made it one of the most practical alloys in marine applications e.g. ship propellers [1, 2]. The microstructure of the alloy consists of a Cu-rich solid solution known as α -phase and β' -phase or martensitic β -phase, surrounded by lamellar eutectoid phase and a series of intermetallic K phases [3, 4]. Among the intermetallic compounds, K_I phase is rosette shape which is rich in Fe, K_{II} phase is smaller than k_I phase and form a dendritic rosette shape which distributed at the α/β boundaries, K_{III} phase is lamellar shape and it forms at the boundary of K_I phase and is rich in Ni and K_{IV} phase is a fine Fe rich precipitations that forms in α phase [5]. Recently, a vast range of investigation have been carried out to study the corrosion behavior of the nickel-aluminum alloy [6, 7] and it has been found that optimum corrosion resistant of the alloy in seawater can be obtained by controlling the microstructure [8]. Corrosion of the bronze alloy in seawater has already been investigated [9], and the tendency of the alloy to corroding was attributed to the formation of β' phase which plays an anodic role compared to α matrix. The complexity of the alloy with several intermetallic phases lead to a significant change in the development of the microstructure, which can result in extensive corrosion resistance in seawater. Results of salt spray test on corrosion behavior of the alloy indicated that corrosion resistance has been improved in the heat treatment sequences like aging, quenching, normalizing and annealing. Characterizing the microstructure showed that quenching transforms all β phase into β' phase and aging results in precipitation of fine K phases. On the other hand, annealing has lead to the transformation of β' martensite into α and K phases [10]. Microstructure of the bronze alloy suffered from cavitation corrosion in seawater showed that the alloy was corroded by selective corrosion at the interface between α phase and intermetallic K precipitates, however, K precipitate-free zones were not considerably corroded. Crevice corrosion of the copper-based alloy was often associated with the formation of a Cu-ion concentration cell and an accelerated attack at the exposed area adjacent to the crevice [11]. Meigh et al. [12] declared crevice corrosion occurs in the nickel-aluminum bronze when it is not cathodically protected. It has been reported that the rate of crevice corrosion of the alloy in seawater is about 0.7-1.0 mmy-1 [13, 14]. The corrosion resistance of the alloy is owned to a protective layer containing both Al and Cu oxides, with 900 to 1000 nm thickness [15, 16]. The Al-rich oxide layer usually forms in the vicinity of the alloy and the Cu-rich forms in the external regions. Oxides of Ni and Fe, and a little Cu salts and Cu hydroxychlorides ($\text{Cu}_2(\text{OH})_3\text{Cl}$ and $\text{Cu}(\text{OH})\text{Cl}$) exist on the surface of the alloy after exposing for long time to seawater. These oxide layers provide corrosion protection by mutually lessening the anodic dissolution reaction, stopping the ionic transport across the oxide layers, and a decrease in the rate of the cathodic reaction on the oxide layers. Despite the fact that there are many studies on the corrosion properties of the alloy in seawater, there has been small number of investigations to study the effect of heat treatment processes on the electrochemical kinetics at the surface of the alloy when it is exposed to seawater environment [17]. For example, Schüssler and Exner [11] conducted a research on the dissolution of a cast nickel-aluminum bronze alloy in seawater with considering a fixed velocity of electrolyte without a considerable contribution on the effect of microstructure on the corrosion. Kear et al. showed that both cathodic [16] and anodic [17] polarization can occur during the corrosion of the alloy in an aqueous solution. The anodic dissolution of the alloy showed significant dissolution of Cu with forming dichlorocuprous anion and the cathodic reaction showed four electron reduction of dissolved oxygen on the surface. The protective nature of the alloy was attributed to the

formation of a Cu_2O layer due to the history of its heat treatment. The reduction of the corrosion rate during the layer formation process was explained by means of the concurrent decrease both of the anodic reaction inside the growing Cu_2O layer, and the cathodic reaction on its surface. Aluminum in passivation was incorporated in the Cu_2O lattice, reducing the rate of oxygen reduction on the Cu_2O surface when the alloy exposed to a corrosive environment [17]. In the present study, the influence of different pre-heat treatments on the passivation behavior of the nickel-aluminum bronze (NAB) alloy was studied using linear polarization [LPR] and impedance [EIS] tests. The effect of different heat treatments on the microstructure development was evaluated by optical microscopy, scanning electron microscopy and X-ray diffraction analysis. The aim of this study was to examine the effect of microstructure on the corrosion behavior of NAB alloy in artificial seawater.

Experimental details

The nickel-aluminum bronze alloy (C95520) was cast according to ASTM B 148 standard and then cut into small pieces of dimensions $6\text{mm}\times 6\text{mm}\times 3.5\text{mm}$. The composition of the alloy was determined by X-ray fluorescence spectrometry (XRF) and it is shown in Table 1.

Table 1. Chemical composition of nickel-aluminum bronze alloy (wt.%) after casting.

Material	Element Composition (wt. %)								
	Cu	Al	Fe	Ni	Si	Pb	Zn	Sn	Mn
Nickel-aluminum bronze alloy (NAB)	Bal.	11.54	4.47	4.60	0.03	0.017	0.002	0.005	0.001

Tensile strength and hardness of the substrate estimated experimentally shown the alloy has tensile strength of about 630 MPa and hardness of 162 HV. The phase composition has been checked at high exposure times by X-ray diffractometry (XRD) in the Bragg-Brentano geometry, using $\text{Cu}=\text{K}\alpha$ radiation ($k=0.15404\text{ nm}$). The specimens were mechanically cleaned, degreased, immersed in an aqueous solution of $20\%\text{HNO}_3$ and then dried and maintained for 24 h in a desiccator in excess of silica gel and in the last part of the cleaning process the alloy weighed. For preparing the aqueous solution, artificial seawater was made according to ASTM D 1141-98 standard. The combination of the compounds in the artificial seawater is given in Table 2.

The artificial seawater with pH of 8.26, dissolved oxygen concentration of around 7.0 ppm and conductivity of 59.8 mS m^{-1} was held at ambient temperature of 27°C during the test. Before accomplishing any corrosion test, the specimens were heat treated in different cycles. The applied heat treatment procedures for altering the microstructure of the alloy are given in Table 3.

Table 2. Chemical composition of artificial seawater based on ASTM D 1141-98 standard.

Component	Quality	Unit
NaHCO ₃	0.201	g/L
CaCl ₂	1.158	g/L
MgCl ₂ ·6H ₂ O	11.112	g/L
SrCl ₂ ·6(H ₂ O)	0.042	g/L
NaCl	25.534	g/L
Na ₂ SO ₄	4.094	g/L
KCl	0.695	g/L
KBr	0.201	g/L
H ₃ BO ₃	0.201	g/L
NaF	0.201	g/L

Table 3. Applied heat treatment cycles to nickel-aluminum bronze alloy.

Heat treatment	Group name	Time (min)	Specimen code	Temperature (°C)
Quenching in water, 27°C	A	15	1	475
			9	675
			17	825
Quenching in water, 27°C	B	30	3	475
			11	675
			19	825
			25	900
Quenching in water, 27°C	C	45	5	475
			13	675
			21	825
Quenching in water, 27°C	D	60	7	475
			15	675
			23	825
Normalizing in air	E	15	2	475
			10	675
			18	825
Normalizing in air	F	30	4	475
			12	675
			20	825
			26	900
Normalizing in air	G	45	6	475
			14	675
			22	825
Normalizing in air	H	60	8	475
			16	675
			24	825

The specimens were mechanically polished with 0.2 μm α -alumina slurry and etched with the solution of 5g FeCl_3 +25 mL HCl +50 mL H_2O . X-ray diffraction test was performed to reveal the intermetallic compounds in the heat treated specimens before and after corrosion tests. To perform the polarization test, the specimens were grinded, polished and degreased with acetone. To prevent other areas from exposing to seawater an area with a dimension of 1mm \times 1mm was chosen and other areas were protected with a polymeric adhesive. The adhesive prepared by combining cure polyamide and reinforcement shielded with BissWax in order to minimize the localized corrosion. General corrosion behavior e.g. oscillation in corrosion potential of the alloy was estimated using linear polarization with EG&G, model 237A corrosion system. The data recorded from this test was analyzed by MATLAB V7.0.0 software. The potential scanning rate was 0.5 mVs^{-1} and when the potential reached to 800 mV, the scan was discontinued. In this test, Ag/AgCl and Pt reference electrodes were used in a potential between -700 and 800 mV setting in maximum value for 0.6 second. The platinum counter electrode enabled controlling the potentiostatic during the test. The recorded values of corrosion rate correspond to the average value from the specimens per exposure time. The passivation resistance layer was estimated with impedance test according to ASTM G 106-89 standard. In the test, potansioestat EG&G, model 273A device was employed and M398 V.1.30 software was used for recording impedance data and drawing Bode curve during the test. To record the data from Nyquist test, Z view-V3.0c software was employed. After linear polarization and impedance test, scanning electron microscope (SEM) was used for characterizing the microstructural changes.

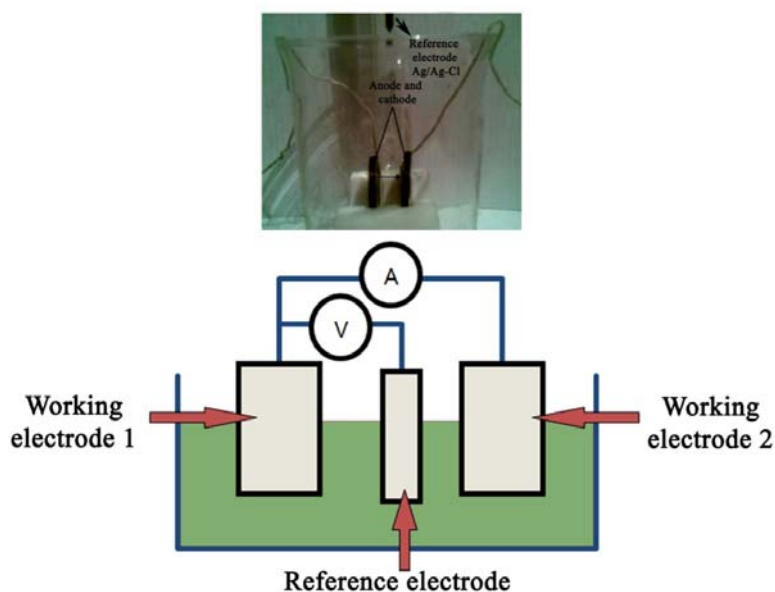


Fig.1. Schematic of the location of the alloy and electrodes in the container filled with artificial seawater.

Results and discussion

The microstructure is characterized by metallographic techniques and is found to consist of α -phase, retained β -phase and numerous K -phases. The microstructures of the specimens before and after heat treatment are shown in Figs.2 and 3, respectively. In the cast alloy, β phase transforms to α phase together with some lamellar K_{III} at grain boundaries and globular star shape K_{II} precipitates. K_{III} is Ni based (usually AlNi) and K_{II} and K_{IV} are a combination of Fe and Al was always emerging as Fe_3Al compound in the microstructure (see Fig.2).

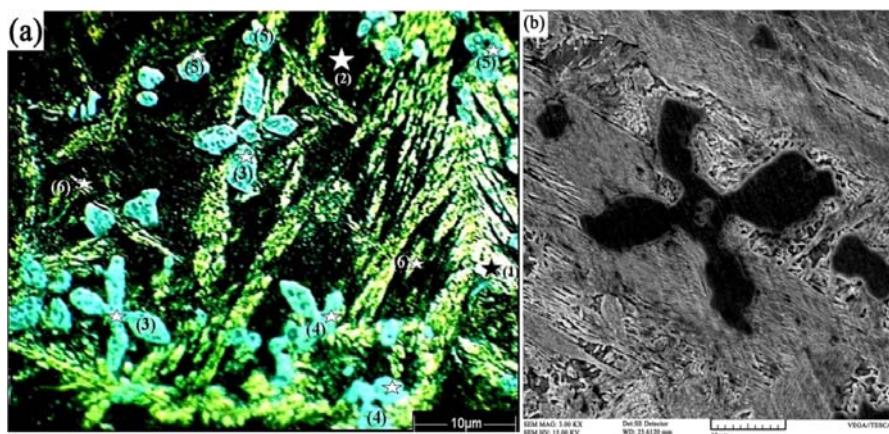


Fig.2. (a) Microstructure of the alloy before heat treatment and corrosion tests and (b) star shape intermetallic at the centre of the non-treated specimen. The numbers in the bracket indicate: (1) α matrix, (2) remained β_2 , (3) K_I , (4) K_{II} , (5) K_{III} and (6) K_{IV} .

Normalizing at a lower temperature causes formation of fine Fe rich K_{IV} within the grains. However, if the cooling was not slow enough, some of the high temperature β was retained as a martensitic structure. The martensite was then transformed into a very fine mixture of α and K phases, with NiAl precipitates, referred to as tempered martensite (see Fig.3).

XRD analysis was performed in one of the specimens normalized at 900°C showing Cu-rich α phase was formed along with K_{III} or K_{IV} in the matrix (Fig.4). It was observed that with increasing the normalizing temperature β phase increased dramatically and eutectoid transformation products together with K phases were decreased. This may in turn affect the products of the reaction with the corrosive environment. Fig.5 shows the microstructure of the alloy after normalizing at 900°C that contains K_{III} and K_{IV} phases formed in the matrix as well as retained β phase.

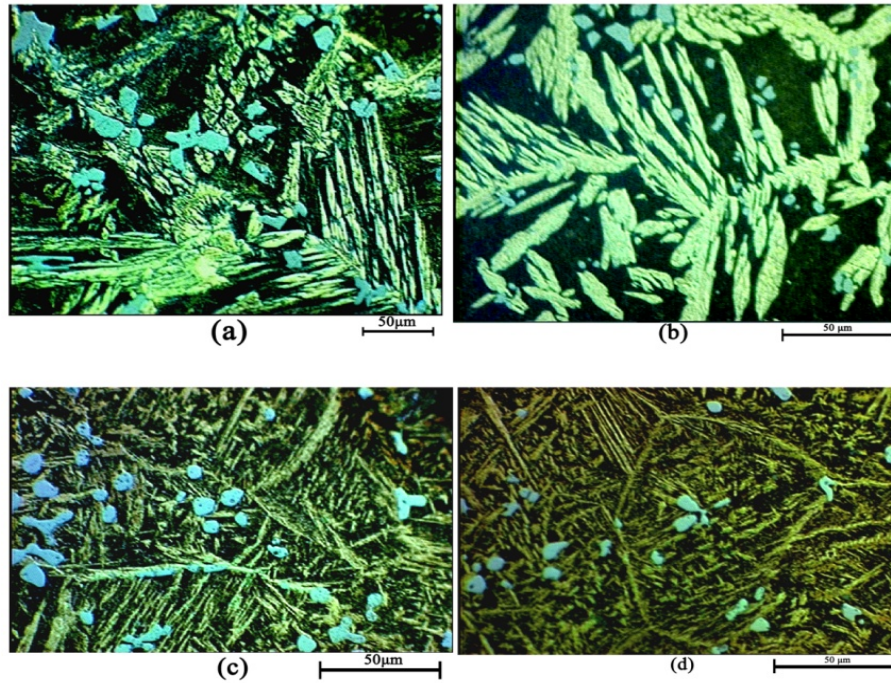


Fig.3. Microstructure of the alloy after normalizing at (a) 475, (b) 675, (c) 825 and (d) 900°C for 30 min.

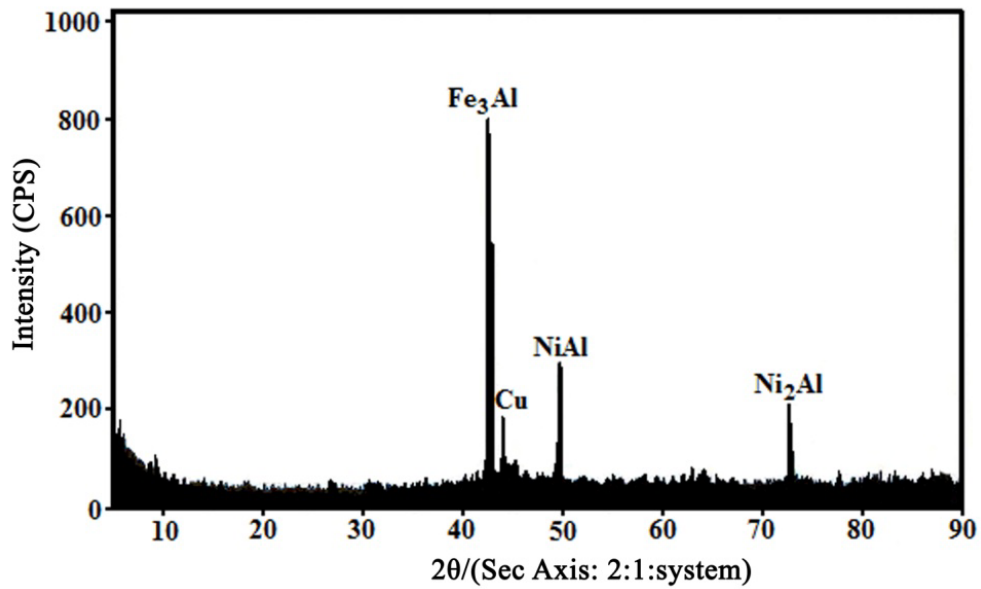


Fig.4. X-ray diffraction from the specimen normalized at 900°C.

When the specimens were air-cooled, more Widmanstatten and α phase have been formed in the matrix. Additionally, after prolonged heat treatment and water quenching, microstructure contained martensite and bainite plus fine eutectoid surrounding the Widmanstatten structure and α phase. For example in the specimen of group A in Table 3, tempering transformed martensite and bainite to a fine eutectoid. As it is seen in Fig.5, when the alloy was air-cooled, Widmanstatten and α phase, eutectoid and traces of bainite and martensite were obviously appeared in the microstructure. However, when the specimens were normalized at 900°C, some of β phase transformed into β' phase, and the other transformed into lamellar α and K intermetallic phases distributing along the boundaries of the alloy. Although martensitic transformation happened during quenching, the microstructure of the alloy still consisted of α , β' and K phases. It was seen that the volume fraction of β' phase increased in the quenched specimens due to the dissolution of both α and K phases.

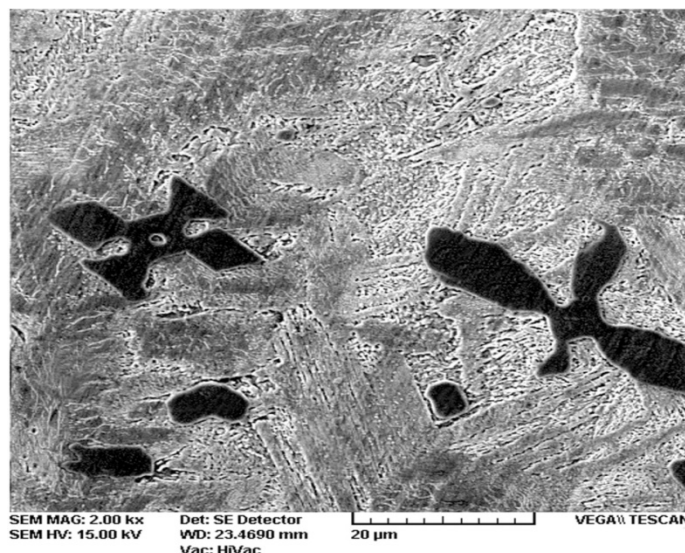


Fig.5. Microstructure of the alloy normalized at 900°C.

Linear polarization test

Fig.6 shows the result of potentiodynamic polarization for the alloy as a function of heat treatment cycle, measured using linear polarization method. The results show a significant similarity in the polarization curves of the specimens heat treated at different heating cycles. It is noted that for the specimen normalized at 675°C for 45 min and then air-cooled (code 14) the polarization resistance was higher than other specimens and its related curve in the polarization diagram shifted to the left side. The results shown in Fig.6 may reflect that the alloy exhibits a higher protective phases in the matrix in the corrosive environment. Although the effect of microstructural difference between intermetallic compounds, primary phases and grain boundary on the corrosion behavior of the metal is not yet well established, the greater polarization resistance of

the specimen with the mentioned condition may indicate that some phases are more resistant to corrosion.

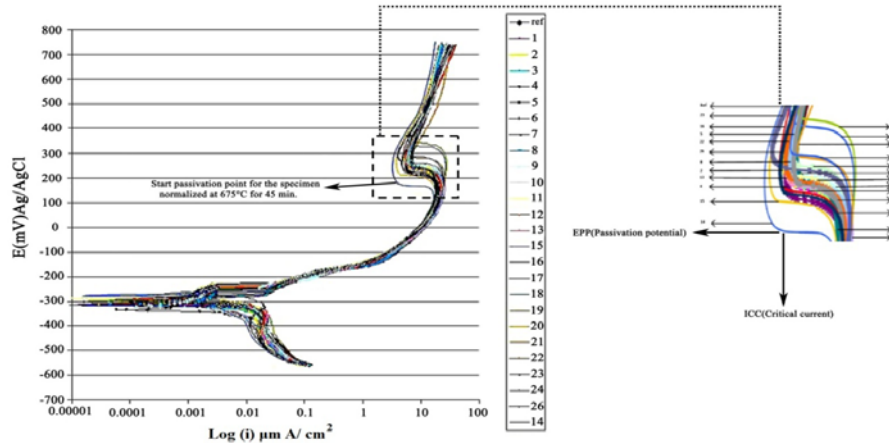


Fig.6. Linear polarization test results for the alloy heat treated in different conditions.

The faster cathodic reaction, resulting from a microstructure with less corrosive phases, was established to associate with the reaction of Fe and Cu atoms with other elements in imperfection sites introduced by the heat treatment cycles. From another point of view, in the alloy subjected to air cooling from high temperatures, a higher dislocation density is anticipated, causing a raise in cathodic reaction rate [18]. Similarly, for the coarsened grained alloy heat treated in lower temperature, the coarsening of Widmanstatten phase produces lower dislocation density, leading to a reduction in cathodic reaction rate and a superior polarization resistance. Furthermore, the presence of Fe showed improvements in corrosion behavior of the alloy. Williams and Komp [19] have reported that an increase in Cu content affected the cathodic polarization behavior in such a way as to reduce the rate of the cathodic reaction in the corrosion process, thereby decreasing corrosion rate. The polarization resistances of the heat treated specimens, however, were higher than that of the non-heat treated alloy. It is obvious that higher Al and Cu contents in the alloy provided by impoverishing some phases offer the beneficial effect on the corrosion resistance as the heat treated alloy (code 14) exhibits greater protective layers on the surface. As it was seen, an especial heat treatment can affect the results of linear polarization in a way that some of them showed high electronic and ionic resistance during the immersion, indicating the products of the corrosion system are more stable and protective. Analysis of the linear polarization curves revealed active-passive behavior for the alloy. After the passive range, rapid increases of current density occurred and passive layer destruction proceeds and following transition into pitting corrosion region is seen for the alloy heat treated with the quenching process. Before this transition, some ephemeral pits formed but were rapidly re-passivated. The main corrosion in this case can be pitting. In contrast, for the substrate subjected to normalizing, i_{corr} increased smoothly with increasing potential and the usual active-passive transition was not appeared. This can be attributed to selective corrosion. It also conceived that commence of passivation was from lower potentials indicating superior specimens for preventing corrosion in artificial seawater

solution. In addition, the normalized specimens exhibited more extended passive behavior in comparison with the quenched specimens. It was also found that the K phases were not attacked, indicating that they were cathodic with respect to the Cu-rich α phase. The continued dissolution of α phase is expected to result in the eventual loss of the K intermetallic compounds. However, it was reported that the corrosion of the alloy in artificial seawater is basically galvanic in nature [20, 21]. The Cu-rich phase was selectively attacked at the interfaces with the intermetallic phases in artificial seawater. Cavitations resulted in a rough surface, containing large size cavities, ductile tearing and grain boundary attack. Microcracks of about 12 μm in length were observed in Cu rich phase adjacent to intermetallic phases. It is believed that selective phase corrosion and cavitation stresses were the main cause of cracking [22]. However, a big doubt about the mechanism of corrosion in the specimens has spurred this investigation to be extended. Hence, extracted results of potentiodynamic curves by Tafel extrapolation are reported in Fig.7. The main results derived from the performed potentiodynamic tests are repeatedly higher corrosion resistance of the normalized specimens compared to the cast and quenched specimens. Noticeably, the superior specimen made up a balance between low current density, low potential and high passive range. When martensite is considered, a high energy level seems to be associated with its resulting microstructure which can significantly affect its corresponding electrochemical behavior. Due to this, it is expected a higher susceptibility to corrosion than those other examined heat-treated specimens. Nonetheless, both martensite structure and volume fraction of dendritic Cu-rich phase were strongly affected by the applied cooling rate intrinsically in each process.

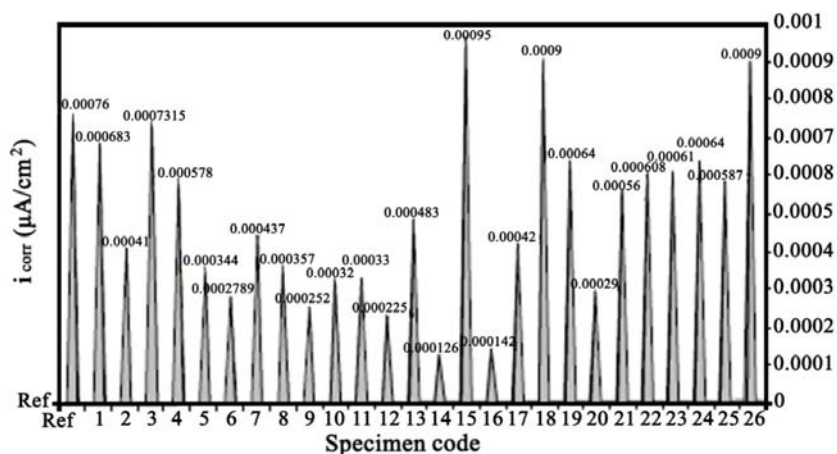


Fig.7. Various corrosion current rate after polarization test.

The effect of heat treating cycles on the polarization characteristics of the alloy depends on the composition of the alloy. With the presence of Cu and Al in the microstructure the polarization has been significantly modified via dissolving the Cu and Al and increasing the Cu content in solid solution. In the alloy, the dissolution of the Ni and Cu rich phases increased the Al contents in solid solution, but did not significantly enhances the passivation power of the surface of the alloy. The similarity

between the polarization curve for the reference specimen and those heat treated seems to support this point. To substantiate the point, the polarization curve for a reference specimen was acquired. By comparison, it can be seen that the curve for the reference specimen and the heat treated specimens were very similar. This point is clearer in the peak current density and the corresponding potential, and also the passive current density, indicating that the anodic polarization behavior of the alloy in the aqueous solution was fundamentally controlled by Cu- and Al-containing phases. Nonetheless, the effect of the heat treatment cycles was obvious by a lower corrosion potential and an inflexion at around 600mV (SCE) in the polarization curve, indicating the preferential dissolution of some elements beyond that potential. It should be mentioned that the differences in Tafel results are attributed to differences in the surface film composition which, in turn, arise from the compositional differences between the alloys heat treated in different cycles. The importance of the effect of the microstructures on the corrosion behavior of the alloy was a significant indication of the influence of heat treatment cycles on the surface morphology evolution. For instance, the signs of corrosion were observed at a very early stage with roughening of the K_I phase. Local attack, however, at the α/K_I boundaries began to take place after six days (see Fig.8). With increasing the immersion time, corrosion products began to appear in α and β matrix, but the corrosion attack was much more rigorous at the active K phases and α/K boundaries. This attack was signaled delineation of grain boundaries at the first stages of corrosion. Moreover, some corrosion products began to appear at the grain boundaries of the specimens normalized at 675°C. Normalizing process reduced the chance of forming local galvanic cells which might exist between different phases, and improved the corrosion resistance of the alloy. The calculated corrosion potential E_{corr} for all specimens indicated a close range between the results leading to an average estimation of about -305/66 mv.

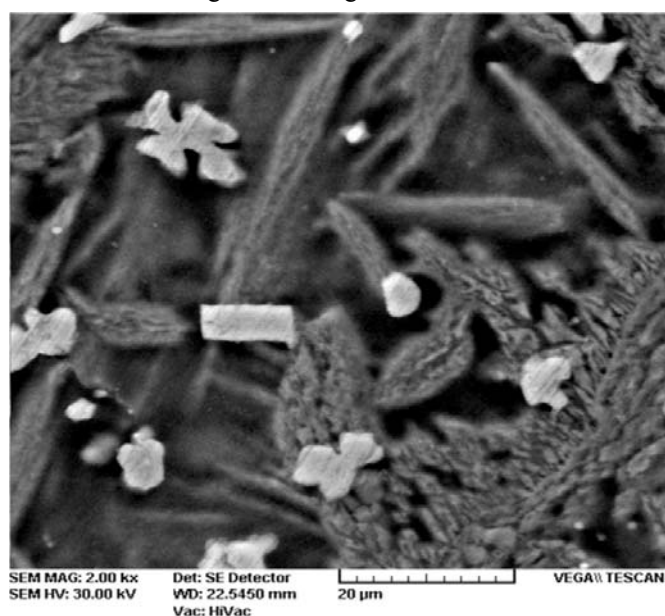


Fig.8. SEM micrographs showing evolution of damage morphology in the specimen normalized at 675°C and immersed in artificial seawater for six days.

For easing the corrosion analysis, some specimens (ref., 3,5,6,12,14,18,20,25 and 26) with highest and lowest i_{corr} were chosen for electrochemical impedance test from the groups shown in Table 3. Each experiment was carried out two times in order to produce more reliable results. The solution resistance (R_s) and the polarization resistance or charge transfer resistance (R_p) were derived using the equivalent circuit model as shown in Fig.9. As it is seen in the model, R_1 is equivalent to R_s . Fig.10 shows the Nyquist plots obtained from AC impedance (EIS) measurement for the specimens immersed in artificial seawater. For plotting the diagrams the corrosion rate (C_R) and corrosion current density (i_{corr}) were calculated from Eqs.1 and 2 in a code written in the software.

$$i_{corr} = \frac{1}{46R_p} \left(\frac{mA}{cm^2} \right) \quad Eq.1$$

$$C_R = 1300 \times \frac{M \cdot i_{corr}}{n \cdot D} (mpy) \quad Eq.2$$

Parameters D , M and n are density (g/cm^3), molecular weight (g/mol) and valence of the alloy, respectively. As can be seen from Fig.10, different behavior can be observed considering all parameters involved in the test. The amount of the polarization resistance taken from the EIS measurement in the alloy depends on the history of heat treatment of the specimens. For instance, R_p value of the normalized specimens at 675°C enhanced in comparison with the quenched specimens.

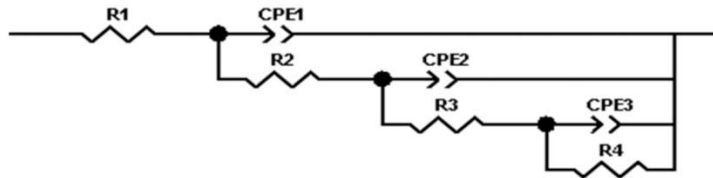


Fig.9. Equivalent electrical circuit model used to derive R_s and R_p .

By comparing the results obtained from different specimens, it can be seen that the Nyquist plots have small polarization resistances at the open circuit potentials. This means that charge transfer process controls the corrosion behavior of the specimens in artificial seawater. The Nyquist plot also clearly shows that the quenching process caused displacing in the left side of the Nyquist plots. It means that the quenching treatment led to a decrease in the impedance of the specimens. However, it is interesting to note that, normalizing the specimens changes the diameter of the semicircles in the Nyquist plots indicating an increase in the value of polarization resistance. Based on the results from the EIS measurement, it can be stated that the normalized alloy (specimen 14) showed the highest corrosion resistance, R_p , compared to other specimens. It should also declare that insignificant changes occurred in the Nyquist plots of some substrates. This might be attributed to the effect of microstructure of the heat treated alloys for absorbing artificial seawater due to dissociation into anions and cations and their involvement to the electrochemical process with increasing the corrosion rate [23].

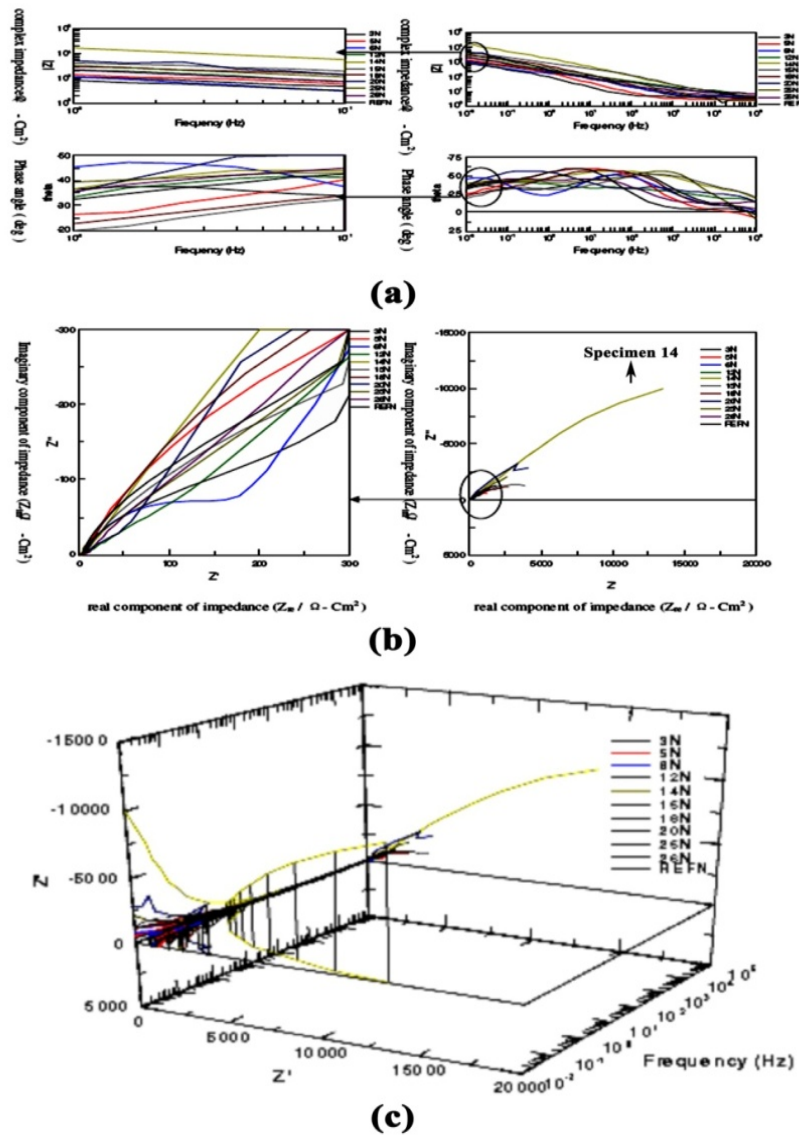


Fig.10. (a) Bode plots, (b) Nyquist plots of the specimens tested in artificial seawater based on the heat treatment histories, obtained from electrochemical impedance spectroscopy test and (c) three dimensional plot relating all parameters involved in the test.

Among the specimens the corrosion rate in the normalized alloy decreased to around 19%. This result can probably be attributed to the supply of oxygen for the Al passivation by artificial seawater and formation of a compact thin layer of Al oxide on its surface and finally reaching to Warburg impedance. However, in the normalizing

process if the temperature reached to 900°C the alloy lost its protection against the corrosive environment. This can be associated with the dissolution of the oxide layer and Cu-rich phase as anodic walls during the corrosion process. The Warburg impedance was created with diffusion process. As the impedance depends on the frequency of the potential perturbation, at high frequencies the Warburg impedance was small since diffusing reactants did not have to move very far. At low frequencies the reactants had to diffuse further, increasing the Warburg-impedance. On the Nyquist plot the Warburg impedance appeared as a diagonal line with a slope of 45° and on the Bode plot, the Warburg impedance exhibited a phase shift of 45°. At the higher normalizing temperature passivation layer resistance had faced with diffusional phenomenon. It means that another resistance circuit, a new one (Z_w), added to the electrical circuit. This can be shown in the electrical circuit with R_p . It is probable the initial time taken to achieve the stabilized potential is associated with the dissolution and conversion of the thermal oxide films. The change from more positive potentials exhibited by the oxides to more negative potentials is due to the changes in the surface films. This process relies on the rate of mass transport for the chloride ion and the cuprous dichloride complex, both of which are engaged in the dissolution of the cuprous oxide. The passivation of the alloy was based on the oxidation of aluminum. It is believed that the aluminum has an enormous affinity for oxygen than other solutes like Cu and always Al_2O_3 is approximately ten times more stable than Cu_2O [5]. However, a single equivalent circuit can be applied where R_s is the solution resistance which in Bode diagram is expressed in a high frequency limit ($F > 1$ Hz), R_l is the passive oxide film resistance and ZCPE is the constant-phase element for the oxide film. On the other hand, as other alternative a complex equivalent circuit consisted with R_s also corresponding to the solution resistance, R_1 and R_2 are the resistances of the porous and barrier layers, respectively [24-27]. For the substrate, thermal oxidation was based on a rapid initial production of Cu_2O at the alloy/oxide interface due to the depletion of Cu. Alumina consequently formed as a protective oxide which was extremely resistant to the passage of cuprous cations which can no longer enter in the layer of cuprous oxide. Providing higher aluminium content by an appropriate thermal cycle can lead to the greater corrosion resistance due to the protective alumina film.

Conclusions

The influence of pre-heat treatment on the corrosion behavior of nickel-aluminum bronze was investigated and the conclusions are as follows:

1. The normalized specimens exhibited significantly lower fractions of pits and better corrosion resistance to artificial seawater in comparison with quenched specimens. Superior specimen showed better corrosion resistance in both short and long term corrosion tests, even better than reference specimen.
2. The corrosion rate of the alloy was dependent on many parameters including the nature of the surface films, the heat treatment process, the alloy composition and the time of immersion in artificial seawater.
3. Polarization plots showed that the Warburg impedance occurred in the passive layer of the specimen normalized at 675°C. The corrosion resistance of the alloy benefited from the microstructure resulted from pre-heat treatment process.

References

- [1] R.C. Barik, J.A. Wharton, R.J.K. Wood, K.S. Tan, K.R. Stokes, Erosion and erosion-corrosion performance of cast and thermally sprayed nickel-aluminium bronze, *Wear*, Vol.259 (2005) pp. 230-242.
- [2] A. Al-Hashem, W. Riad, The role of microstructure of nickel-aluminium-bronze alloy on its cavitation corrosion behavior in natural seawater, *Materials Characterization*, Vol.48 (2002) pp.37- 41.
- [3] F. Hasan, J. Iqbal, N. Ridley, Microstructure of As-cast aluminum bronze containing iron, *Materials Science and Technology*, Vol.1 (1985) p.312.
- [4] F. Hasan, A. Jahanafrooz, G.W. Lorimer, N. Ridley, The morphology, crystallography, and chemistry of phases in As-cast nickel-aluminum-bronze, *Metallurgical and Materials Transactions A*, Vol.13A (1982) p.1337.
- [5] J.A. Wharton, R.C. Brik, G. Kear, R.J.K. Wood, K.R. Stokes, F.C. Walsh, The corrosion of nickel-aluminum bronze in seawater, *Corrosion Science*, Vol.47(2005) pp.3336-3367.
- [6] J.A. Wharton, K.R. Stokes, The influence of nickel-aluminum bronze microstructure and crevice solution on the initiation of crevice corrosion, *Electrochimica Acta*, Vol.53 (2008) pp.2463-2473.
- [7] M.D. Fuller, S. Swaminathan, A.P. Zhilyaev, T.R. McNelley, Microstructural transformations and mechanical properties of cast NiAl bronze: Effects of fusion welding and friction stir processing, *Materials Science and Engineering A*, Vol.463(2007) pp.128-137.
- [8] H.S. Campbell, Aluminium bronze corrosion resistance guide, Publication 80, Copper Development Association, UK (July 1981), pp. 1-27.
- [9] Zanis Charlws, J. Ferrara Robert, Sea water corrosion of nickel-aluminum bronze, *Transactions of the American Foundrymen's Society*, Vol.82 (1974) pp.71-78.
- [10] Chen Rui-Ping, Liang Ze-Qin, Zhang Wei Wen, Zhang Da-Tong, Luo Zong-Qiang, Li Yuan-Yuan, Effect of heat treatment on microstructure and properties of hot-extruded nickel-aluminum bronze, *The Transactions of Nonferrous Metals Society of China*, Vol.17 (2007) pp.1254-1258.
- [11] A. Schussler, H.E. Exner, The corrosion of nickel-aluminium bronzes in seawater-I. Protective layer formation and the passivation mechanism, *Corrosion Science*, Vol.34 (1993) p.1793.
- [12] H. Meigh, Cast and wrought aluminium bronzes- properties, Processes and Structure, 1st ed., IOM Communications, (2000).
- [13] F.L. LaQue, Marine corrosion, Wiley, New York, (1975).
- [14] J.C. Rowlands, Studies of the preferential phase corrosion of cast nickel aluminium bronze in seawater, in: Proc. 8th Inter. Cong. Metallic Corros., (1981), p.1346.
- [15] G. Kear, B.D. Barker, K.R. Stokes, F.C. Walsh, Electrochemical corrosion of unalloyed co in chloride media-a critical review, *Corrosion Science*, Vol.47 (2004) p.1694.
- [16] G. Kear, B.D. Barker, K.R. Stokes, F.C. Walsh, Electrochemical corrosion behaviour of 90-10Cu-Ni alloy in chloride-based electrolytes, *Journal of Applied Electrochemistry*, Vol.34 (2004) p.659.

- [17] G. Kear, B.D. Barker, F.C. Walsh, Electrochemistry of non-aged 90-10 copper-nickel alloy (UNS C70610) as a function of fluid flow Part 1: Cathodic and anodic characteristics, *Electrochimica Acta*, Vol.52 (2007) pp.1889-1898.
- [18] Her-Hsiung Huang, Wen-Ta Tsai and Ju-Tung Lee, The influences of microstructure and composition on the electrochemical behavior of a516 steel weldment, *Corrosion Science*, Vol. 36, No.6 (1994) pp. 1027-1038.
- [19] F.T. Cheng, K.H. Lo, H.C. Man, An electrochemical study of the crevice corrosion resistance of NiTi in Hanks' solution, *Journal of Alloys and Compounds*, Vol.437 (2007), pp.322-328.
- [20] E.A. Culpán, R. Rose, Corrosion behaviour of cast nickel aluminum bronze in sea water, *Britain Corrosion Journal*, vol.14 Issue 3 (1979) p.160.
- [21] G.W. Loriner, F. Hasan, J. Iqbal, N. Ridley, Observation of microstructure and corrosion behaviour of some aluminum bronzes, *Britain Corrosion Journal*, Vol. 21 Issue 4 (1986) pp.244-247.
- [22] A. Al-Hashem, W. Riad, The role of microstructure of nickel-aluminium-bronze alloy on its cavitation corrosion behavior in natural seawater, *Materials Characterization*, vol.48 (2002) pp.37-41.
- [23] H. Jafari, M. Hasbullah Idris, A. Ourdjini, H. Rahimi, B. Ghobadian, EIS study of corrosion behavior of metallic materials in ethanol blended gasoline containing water as a contaminant, *Fuel*, Vol.90 Issue 3 (March 2011) pp.1181-1187.
- [24] WR. Osório, LC. Peixoto, MV. Canté, A. Garcia, Electrochemical corrosion characterization of Al-Ni alloys in a dilute sodium chloride solution, *Electrochimica Acta*, vol. 55 (2010) pp.4078-85.
- [25] WR. Osório, LC. Peixo, DJ. Moutinho, LG. Gomes, IL. Ferreira, A. Garcia, Corrosion resistance of directionally solidified Al-6Cu-1Si and Al-8Cu-3Si alloys castings, *Materials and Design*, vol.32 (2011) pp.3832-7.
- [26] WR. Osório, LC. Peixoto, MV. Canté, A. Garcia, Microstructure features affecting mechanical properties and corrosion behavior of a hypoeutectic Al-Ni alloy, *Materials and Design*, vol.31 (2010) pp.4485-9.
- [27] WR. Osório, DM. Rosa, LC. Peixoto, A. Garcia, Cell/dendrite transition and electrochemical corrosion of Pb-Sb alloys for lead-acid battery applications, *Journal of Power Sources*, vol. 196 Issue15 (2011) pp. 6567-6572.